

physica status solidi

www.pss-journals.com

reprint



Fidelity of optically induced single-spin rotations in semiconductor quantum dots in the presence of nuclear spins

Julia Hildmann and Guido Burkard*

Department of Physics, University of Konstanz, 78457 Konstanz, Germany

Received 19 December 2013, revised 25 February 2014, accepted 27 February 2014

Published online 4 April 2014

Keywords coherent control, hyperfine interaction, semiconductor quantum dots, nuclear spin, spin qubits

* Corresponding author: e-mail guido.burkard@uni-konstanz.de, Phone: +49 7531 885256, Fax: +49 7531 3760



This is an open access article under the terms of the Creative Commons Attribution License, which permits use, distribution and reproduction in any medium, provided the original work is properly cited.

We examine the influence of nuclear spins on the performance of optically induced rotations of single electron spins in semiconductor quantum dots. We consider Raman-type optical transitions between electron spin states and take into account the additional effect of the Overhauser field. We calculate average

fidelities of rotations around characteristic axes in the presence of nuclear spins analytically with perturbation theory up to second order in the Overhauser field. Moreover, we calculate the fidelity using numerical averaging over the nuclear field distribution, including arbitrary orders of the hyperfine interaction.

1 Introduction Single electron spins in quantum dots represent a suitable physical system for the experimental realization of quantum bits (qubits) [1]. Since single- and two-qubit operations are sufficient for implementing any arbitrary quantum gate [2], a large amount of research has been conducted for the realization of single-qubit state control and two-qubit operations [3–9]. Along with electrical control, one of the possibilities of manipulating single electron spin states is by optical means [4, 10, 11, 14], which offers a fast and coherent way for control of spin states in quantum dots. Experimental achievements in optical initialization, read out, coherent control, and manipulation of single electron spins in quantum dots [15–22] have reached a level at which their use for quantum information processing seems to be feasible. Additionally, optical control offers the possibility of incorporating electron spin qubits into hybrid systems in which the single-spin state is entangled with the state of a photon and quantum information is transferred by photons [23–25]. The accomplishment of the essential steps for optimal optical single-spin control is affected by different types of errors. One type of error can be caused by imperfection of the applied laser pulses, which can be optimized by using laser feedback loops [11] or laser pulses of specific form [12, 13]. Another type of error can originate from mixing of heavy- and light-hole states. It influences the trion state, which is used in some schemes as an intermediate state

[14, 22] and can result in an actual population of the trion state and not a virtual one, which is necessary for the control schemes. However, the mixing of the heavy and light holes in quantum dots can be controlled, e.g., by means of anisotropic stress [26] and in this way the errors created by the phenomenon can be avoided.

An additional intrinsic mechanism causing decoherence of electron spins in III–V semiconductor quantum dots is their interaction with the nuclear spins of the host material [7, 27–29]. An electron confined in such a quantum dot interacts by hyperfine coupling with a large nuclear bath (roughly 10^5 – 10^6 nuclear spins per quantum dot). The total magnetic field of the nuclei, also called the Overhauser field, fluctuates randomly and acts as an effective magnetic field on the electron, causing dephasing of the electron spin state. There are possibilities of improving the decoherence time by reducing the fluctuations of the Overhauser field. One such possibility is to polarize nuclear spins to a high degree [28]; another is to drive or project the nuclear spin state into an eigenstate of the Overhauser field operator [30, 31]. A significant improvement of electron spin coherence time was observed in experiments where nuclear spin fluctuations were suppressed by driving the nuclear field to a stable state [32–34].

In this paper, we focus on the single-spin rotation errors arising from the interaction with an unpolarized ensemble of nuclear spins. One possibility of rotating the single-spin

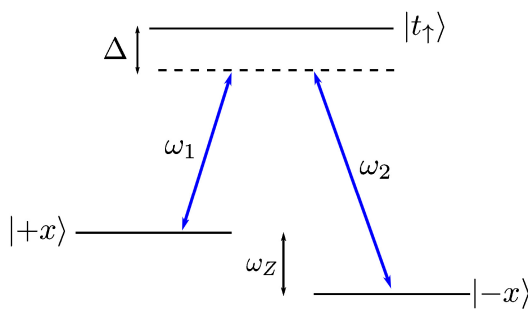


Figure 1 Energy level scheme for an electron spin interacting with σ_+ -polarized light. The transverse magnetic field splits x -eigenstates of the electron spin by the Zeeman energy ω_Z . The electron spin states are virtually coupled to the trion state $|t_\uparrow\rangle$ by the laser pulses $\Omega_1(t)$ and $\Omega_2(t)$ with frequencies ω_1 and ω_2 , with detuning Δ .

states in a quantum dot is by using Raman transitions [4, 10] between single electron spin states split by a magnetic field in Voigt geometry via the trion state comprised of two electrons and a heavy hole. In this case, the transitions are driven by specifically detuned laser pulses (Fig. 1). The hyperfine interaction leads to a fluctuating spin-state splitting and therefore to imperfect spin rotations.

To compare the single-spin rotations in the presence and in the absence of nuclear spins, we compute the fidelities of the unitary time evolution of the electron spin state under the action of the laser light with and without including the hyperfine interaction. We average the obtained fidelities over the Overhauser field distribution analytically to second order of the hyperfine coupling and numerically to an arbitrary order. We calculate the average fidelities for rotation axes parallel and perpendicular to the external magnetic field and discuss the factors that influence the average rotation fidelities in both cases. The single-qubit gate errors are an important parameter to estimate the performance of quantum error correction [35]. Some standard estimates predict that fault-tolerant quantum computation requires a fidelity of at least 0.9999.

The investigation of the fidelities of single-qubit rotations exposes the dependence on the relative orientation of the rotation axis relative to the external magnetic field. We find that the errors of electron spin state rotations around different axes are not identical. It would be interesting to confirm this observation for electron spin resonance on single spins in electrostatically defined or semiconductor nanowire quantum dots.

We find an oscillatory behavior of the fidelity, which, in contrast to the case of cavity-mediated two-qubit gates [36], depends only on the interaction time, the Rabi frequencies of the composite laser pulse, and the detuning. This allows us to find an analytical description of the oscillatory behavior as a function of time, and investigate the recurrence of unit fidelity at finite gate times. These recurrences could be used for optimized gate operation in the presence of hyperfine interactions.

This paper is organized as follows. In Section 2, we describe the mechanism of Raman-type optical transitions

between single electron states. We include the hyperfine interaction to the system in Section 3 and derive the time-evolution operator of the single-spin state in the presence of the Overhauser field. We present the calculated rotation fidelities with the analysis of the oscillatory behavior and possible experimental observation of the calculated effects in Section 4.

2 Optically-induced single-spin rotations

The interaction between σ_+ -polarized light in the growth direction z and a single electron confined in a quantum dot is given by

$$H = E_t |t_\uparrow\rangle \langle t_\uparrow| + g^*(t) |t_\uparrow\rangle \langle \uparrow| + g(t) |\uparrow\rangle \langle t_\uparrow|, \quad (1)$$

where $|\uparrow\rangle$ is the spin-up state in the conduction band and $|t_\uparrow\rangle$ is the trion state formed by two electrons in the singlet state and a heavy hole with angular momentum $+3/2$. E_t is the energy of the trion state and $g(t)$ is the coupling to the laser field. With an additional magnetic field applied in the x direction, perpendicular to the growth direction (Voigt geometry), the Hamiltonian (1) reads in the basis $|\pm x\rangle = \frac{1}{\sqrt{2}}(|\uparrow\rangle \pm |\downarrow\rangle)$, $|t_\uparrow\rangle$ [23]

$$H = \begin{pmatrix} \frac{\omega_Z}{2} & 0 & \frac{g^*(t)}{\sqrt{2}} \\ 0 & \frac{-\omega_Z}{2} & \frac{g^*(t)}{\sqrt{2}} \\ \frac{g(t)}{\sqrt{2}} & \frac{g(t)}{\sqrt{2}} & E_t \end{pmatrix}, \quad (2)$$

where ω_Z is the Zeeman splitting of the electron states $|\pm x\rangle$. Applying two-color laser pulses enables arbitrary rotation of the electron spin by a single pulse [10],

$$g(t) = \Omega_1(t)e^{-i\omega_1 t - i\alpha} + \Omega_2(t)e^{-i\omega_2 t},$$

with Raman resonance conditions:

$$\omega_1 + \omega_Z/2 = \omega_2 - \omega_Z/2 = E_t - \Delta,$$

where Δ is the laser detuning from the trion resonance (see Fig. 1) and α gives the relative phase between two lasers with real Rabi frequencies $\Omega_1(t)$ and $\Omega_2(t)$. In the rotating frame given by $e^{i\omega_Z t/2} |\pm x\rangle$, $e^{-i(E_t - \Delta)t} |t_\uparrow\rangle$, the Hamiltonian is

$$\begin{aligned} H = & \Delta |t_\uparrow\rangle \langle t_\uparrow| \\ & + \frac{1}{\sqrt{2}} (\Omega_1(t)e^{i\alpha} + \Omega_2(t)e^{i\omega_Z t}) |+x\rangle \langle t_\uparrow| + h.c. \\ & + \frac{1}{\sqrt{2}} (\Omega_1(t)e^{i\alpha - i\omega_Z t} + \Omega_2(t)) |-x\rangle \langle t_\uparrow| + h.c. \end{aligned} \quad (3)$$

In the case $|\Omega_{1,2}(t)| \ll \omega_Z$, the fast oscillating terms can be neglected and the Hamiltonian becomes

$$\begin{aligned} H = & \Delta |t_\uparrow\rangle \langle t_\uparrow| + \frac{1}{\sqrt{2}} \Omega_1(t)e^{i\alpha} |+x\rangle \langle t_\uparrow| + h.c. \\ & + \frac{1}{\sqrt{2}} \Omega_2(t) (|-x\rangle \langle t_\uparrow| + |t_\uparrow\rangle \langle -x|). \end{aligned} \quad (4)$$

This Hamiltonian describes the Λ system presented in Fig. 1. If the temporal profiles of the laser pulses for $\Omega_1(t)$ and $\Omega_2(t)$ are of rectangular shape and of the same width, the Hamiltonian (4) will be proportional to a step function, such that the time dependance of the Rabi frequencies can be omitted. For a realistic laser pulse, this assumption holds if the rise time of the pulse is much shorter than its duration. Assuming $|\Omega_{1/2}| \ll \Delta$, we obtain the effective Hamiltonian by the Schrieffer–Wolff transformation [4, 36]:

$$H_{\text{eff}} \approx \begin{pmatrix} -\frac{\Omega_1^2}{2\Delta} & -e^{i\alpha} \frac{\Omega_1 \Omega_2}{2\Delta} & 0 \\ -e^{-i\alpha} \frac{\Omega_1 \Omega_2}{2\Delta} & -\frac{\Omega_2^2}{2\Delta} & 0 \\ 0 & 0 & \Delta + \frac{\Omega_1^2 + \Omega_2^2}{2\Delta} \end{pmatrix}.$$

The electron spin states are decoupled from the trion state and the effective single-spin Hamiltonian reads

$$H_{\text{eff}} = \frac{\Omega_2^2 - \Omega_1^2}{4\Delta} \sigma_z - \cos \alpha \frac{\Omega_1 \Omega_2}{2\Delta} \sigma_x + \sin \alpha \frac{\Omega_1 \Omega_2}{2\Delta} \sigma_y, \quad (5)$$

where σ_i are the Pauli matrices in the basis of the states $|\pm x\rangle$. The time-evolution operator for the Hamiltonian (5) can be represented as

$$U(t) = \exp(-i\omega t \hat{n} \cdot \boldsymbol{\sigma}),$$

where

$$\omega = \frac{\Omega_1^2 + \Omega_2^2}{4\Delta},$$

where $\boldsymbol{\sigma}$ is the vector of Pauli matrices and the components of the unit vector \hat{n} are given by

$$\begin{aligned} n_x &= -\cos \alpha \frac{2\Omega_1 \Omega_2}{\Omega_1^2 + \Omega_2^2} \equiv -\cos \alpha n_{\perp}, \\ n_y &= \sin \alpha \frac{2\Omega_1 \Omega_2}{\Omega_1^2 + \Omega_2^2} \equiv \sin \alpha n_{\perp}, \\ n_z &= \frac{\Omega_2^2 - \Omega_1^2}{\Omega_1^2 + \Omega_2^2}. \end{aligned}$$

3 Hyperfine coupling To study the influence of nuclear spins on the performance of the spin rotations, we add the hyperfine interaction of an electron confined in a quantum dot to the Hamiltonian (1), which is given by the contact Fermi interaction [29]:

$$H_{\text{hf}} = \mathbf{S} \cdot \mathbf{h} = \mathbf{S} \cdot \sum_{k=0}^N A_k \mathbf{I}_k, \quad (6)$$

where \mathbf{S} is the electron spin operator and \mathbf{h} is the so-called Overhauser field, the effective nuclear spin field, \mathbf{I}_k are the nuclear spin operators, A_k is the hyperfine coupling strength

of a nuclear spin at the k th lattice site, and N is the number of nuclear spins interacting with the electron. According to the central limit theorem, the expectation value of the Overhauser field underlies a Gaussian distribution with average value of zero and with the standard deviation $\sigma = A/\sqrt{N}$, where A is the average hyperfine constant. For our calculations, we used $A = 90 \mu\text{eV}$ and $N = 10^5$ [7].

The system Hamiltonian together with the hyperfine interaction is

$$H^h = \begin{pmatrix} \frac{\omega_z}{2} + \frac{h_x}{2} & \frac{(h_z + ih_y)}{2} & \frac{g^*(t)}{\sqrt{2}} \\ \frac{(h_z - ih_y)}{2} & \frac{-\omega_z}{2} - \frac{h_x}{2} & \frac{g^*(t)}{\sqrt{2}} \\ \frac{g(t)}{\sqrt{2}} & \frac{g(t)}{\sqrt{2}} & E_t \end{pmatrix}, \quad (7)$$

where h_i ($i = x, y, z$) are the components of the Overhauser field, which is considered here to be a fluctuating effective magnetic field. We express the Hamiltonian (7) in the same rotating frame as for the Hamiltonian (3), and neglect again the fast oscillating terms under the assumption $|\Omega_{1,2}(t)|, \sigma \ll \omega_z$. In this way, the transverse terms from the hyperfine coupling are excluded from our calculations and the Hamiltonian in the rotating frame with included Overhauser field becomes

$$H^h \simeq \begin{pmatrix} \frac{h_x}{2} & 0 & \frac{\Omega_1(t)e^{i\alpha}}{\sqrt{2}} \\ 0 & \frac{-h_x}{2} & \frac{\Omega_2(t)}{\sqrt{2}} \\ \frac{\Omega_1(t)e^{-i\alpha}}{\sqrt{2}} & \frac{\Omega_2(t)}{\sqrt{2}} & \Delta \end{pmatrix}. \quad (8)$$

Choosing again the laser profiles of rectangular shape and the same width for $\Omega_{1/2}(t)$ and assuming that the Overhauser field is static, we can render the Hamiltonian H^h time independent. The system undergoes the dynamics given by H^h only during the laser pulse. Applying again the Schrieffer–Wolff transformation and treating the nuclear field as an effective magnetic field, we obtain an effective Hamiltonian. Also here, the electron spin states are decoupled from the trion state and we can work only on the electron spin state subspace. For the single-spin Hamiltonian, we find (up to a constant)

$$\begin{aligned} H_{\text{eff}}^h &\approx \frac{1}{2} \left(h_x - \frac{\Omega_1^2(t)}{2\Delta - h_x} + \frac{\Omega_2^2(t)}{2\Delta + h_x} \right) \sigma_z \\ &- \cos \alpha \frac{2\Delta \Omega_1(t) \Omega_2(t)}{4\Delta^2 - h_x^2} \sigma_x \\ &+ \sin \alpha \frac{2\Delta \Omega_1(t) \Omega_2(t)}{4\Delta^2 - h_x^2} \sigma_y. \end{aligned} \quad (9)$$

The unitary time-evolution operator of this Hamiltonian can be represented as

$$U_h(t) = \exp(-i\omega(h)t \hat{n}(h) \cdot \boldsymbol{\sigma}), \quad (10)$$

where

$$\begin{aligned} \omega(h) = \frac{1}{2(4\Delta^2 - h_x^2)} & \left(16\Delta^2\Omega_1^2\Omega_2^2 + (2\Delta(\Omega_2^2 - \Omega_1^2) \right. \\ & \left. - h_x(\Omega_2^2 + \Omega_1^2) + h_x(4\Delta^2 - h_x^2) \right)^{1/2}. \end{aligned}$$

The components of the unit vector $\hat{n}(h)$ are

$$n_x(h) = -\cos\alpha n_{\perp}(h),$$

$$n_y(h) = \sin\alpha n_{\perp}(h),$$

$$n_z(h) = \frac{2\Delta(\Omega_2^2 - \Omega_1^2) - h_x(\Omega_2^2 + \Omega_1^2) + h_x(4\Delta^2 - h_x^2)}{2(4\Delta^2 - h_x^2)\omega(h)},$$

with

$$n_{\perp}(h) \equiv \frac{2\Omega_1\Omega_2\Delta}{(4\Delta^2 - h_x^2)\omega(h)}.$$

4 Fidelity The deviation in the optical rotations of the electron spin state due to the coupling to nuclear spins is studied by calculating the fidelity of the time evolution. The fidelity for two unitary operators averaged over all possible initial states on which the operators are acting is given by [37, 38]

$$\mathcal{F} = \frac{n + |\text{Tr}[U_{\text{ideal}}^\dagger U_{\text{actual}}]|^2}{n(n+1)}, \quad (11)$$

where n is the dimension of the Hilbert space, U_{ideal} represents the ideal operator, and U_{actual} is the actual operator. The fidelity of single-spin rotation ($n = 2$) in the presence of nuclear spins is given by

$$\mathcal{F} = \frac{1}{3} + \frac{1}{6} |\text{Tr}[U(t)^\dagger U_h(t)]|^2.$$

The trace of the product of the perfect time-evolution operator and the time-evolution operator with random Overhauser field is given by

$$\begin{aligned} \text{Tr}[U(t)^\dagger U_h(t)] = 2(\cos\omega t \cos\omega(h)t) \\ + \sin\omega t \sin\omega(h)t[n_{\perp}n_{\perp}(h) + n_zn_z(h)]. \end{aligned}$$

To obtain the average fidelity, we need to average the following expression analytically to a particular order or numerically over the Overhauser field distribution:

$$\begin{aligned} \mathcal{F} = \frac{1}{3} + \frac{2}{3} (\cos\omega t \cos\omega(h)t) \\ + \sin\omega t \sin\omega(h)t[n_{\perp}n_{\perp}(h) + n_zn_z(h)]^2. \quad (12) \end{aligned}$$

The average fidelity to the second order of the Overhauser field is given by

$$\begin{aligned} \langle \mathcal{F} \rangle_h = 1 - \frac{(\Omega_1^2 + \Omega_2^2 - 4\Delta^2)^2(\Omega_1^2 - \Omega_2^2)^2}{96\Delta^4(\Omega_1^2 + \Omega_2^2)^2} t^2\sigma^2 \\ - \frac{2(\Omega_1^2 + \Omega_2^2 - 4\Delta^2)^2\Omega_1^2\Omega_2^2}{3\Delta^2(\Omega_1^2 + \Omega_2^2)^4} \sigma^2 \sin^2\omega t + \mathcal{O}(\sigma^4), \end{aligned} \quad (13)$$

where $\sigma = \langle h_x^2 \rangle$ is the standard deviation of the Overhauser field distribution. The numerically obtained average fidelity using the effective Hamiltonians is presented in comparison to the analytical result to second order of hyperfine interaction in Figs. 2 and 3.

Additionally, we determine the exact average fidelity by evaluating Eq. (11) for the full three-level system. In this case, the ideal unitary time-evolution operator is defined through the Hamiltonian (4) and the actual unitary time-evolution operator is defined through the Hamiltonian (8). The averaging of the fidelity over the Overhauser field is done numerically.

Figure 2a shows the average fidelity for a rotation around a generic axis, which is not parallel or perpendicular to the characteristic axes. In this case, $\Omega_1 \neq \Omega_2$ and $\Omega_{1,2} \neq 0$, as can be seen in Eqs. (5) and (9). For the parameters $\Omega_1 = 1$ meV, $\Omega_2 = 0.5$ meV, and $\Delta = 10$ meV, the duration of a $\pi/2$ rotation in the effective model is 35 ps and the average fidelity is 0.999978 (the exact model gives 0.999988 for a pulse duration of 35 ps). The average fidelities obtained both numerically and using second-order perturbation theory from the effective model, Eq. (13), agree for short interaction times and remain in good agreement up to the nanosecond scale. However, the agreement between the average fidelities calculated using the effective Hamiltonians and the exact average fidelity is presented up to 50–100 ps.

The rotations around the axis along the magnetic field (x -axis here) are obtained by setting Ω_1 or Ω_2 equal to zero. The average fidelity for such a rotation is shown in Fig. 2b with $\Omega_1 = 1$ meV, $\Omega_2 = 0$, and $\Delta = 10$ meV. For these parameters, a $\pi/2$ rotation in the effective single-spin model lasts around 41 ps and the average error for the rotation is $1 - \langle \mathcal{F} \rangle_h = 5.3 \times 10^{-5}$ (the exact average fidelity for a laser pulse of 41 ps duration is $1 - \langle \mathcal{F} \rangle_h = 3.9 \times 10^{-5}$). The reduction of the average fidelity in this case is anticipated, since the rotation frequency ω is a quadratic function of both Rabi frequencies and the reduction of these frequencies leads to smaller ω and thus to smaller fidelities. The average fidelity obtained analytically to second order of the Overhauser field coincides with the numerically averaged fidelity for a few full rotations around the x -axis (Fig. 2b) and reproduces it on the nanosecond scale.

The rotations around an axis lying in the y – z plane (corresponding to the σ_x and σ_y terms in Eqs. (5) and (9)) can be obtained by applying pulses with $\Omega_1 = \Omega_2$. Furthermore,

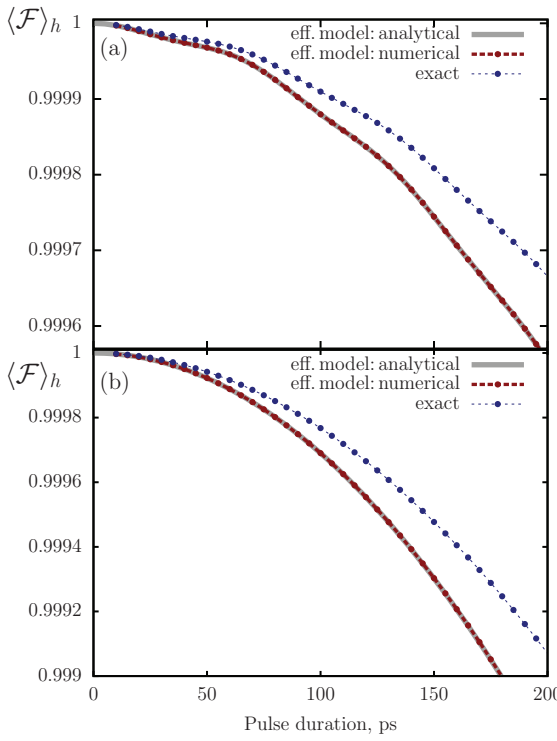


Figure 2 (a) Fidelity averaged over Overhauser field for a generic spin rotation. The presented results were obtained numerically and analytically from the effective two-state model and compared to average fidelity calculated exactly considering all three electronic levels. Here, $\Omega_1 = 1$ meV, $\Omega_2 = 0.5$ meV, and $\Delta = 10$ meV. (b) Fidelity for a spin rotation around the x -axis for the effective single-spin model averaged numerically over Overhauser field distribution and its the average value to second order of the Overhauser field. The exact average fidelity is obtained from exact dynamics of the three-level electronic system. Here, $\Omega_1 = 1$ meV, $\Omega_2 = 0$, and $\Delta = 10$ meV.

the rotation axis is specified by the phase α , as shown in Eq. (5). However, setting $\Omega_1 = \Omega_2$ does not result in a rotation around an axis lying in the $y-z$ plane if the electron spin interacts with the nuclear spins. The axis is rotated out of the $y-z$ plane because of the Overhauser field, as can be seen in Eq. (9). The average fidelity of a single-spin rotation around an axis, that is defined by $\Omega_1 = 1$ meV and $\Omega_2 = 0.98$ meV, is shown in Fig. 3. The fidelity averaged over the nuclear spin distribution numerically to an arbitrary order and averaged analytically to the second order of the Overhauser field h is enhanced compared to the average fidelities in other cases presented in Fig. 2. The same can be found also for the exact average fidelity (Figs. 2 and 3). A good agreement between the exact average fidelity and the average fidelity computed using the effective model can be observed on the nanosecond time scale. The duration of a $\pi/2$ rotation in the effective model reduces to 20 ps, while the average error for such rotation decreases to $1 - \langle \mathcal{F} \rangle_h = 3 \times 10^{-6}$ (the exact value is $1 - \langle \mathcal{F} \rangle_h = 4 \times 10^{-9}$). This strong improvement in fidelity cannot be explained only by increase of the inter-

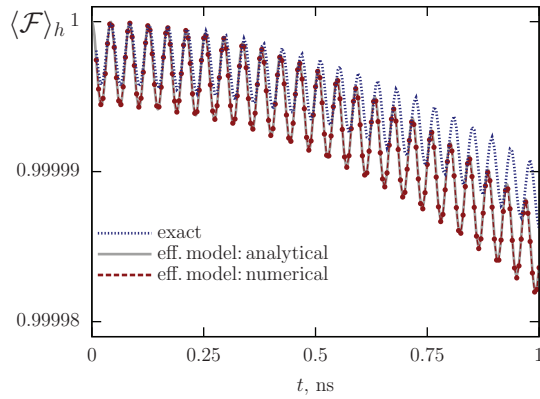


Figure 3 Fidelity for rotations around an axis nearly in the $y-z$ plane averaged over nuclear spins numerically and to second order of hyperfine interaction using the effective single-spin model. The exact average fidelity was computed numerically without excluding the trion level. Used parameters: $\Omega_1 = 1$ meV, $\Omega_2 = 0.98$ meV, and $\Delta = 10$ meV.

action energy with the laser light ω . The increased average fidelity in the case when Ω_1 is close to Ω_2 and vice versa can be attributed to the interplay of different contributions leading to a reduction of the average fidelity. As can be seen in Eq. (13), the second term reduces the fidelity as $\propto t^2$ and the third term as $\propto \sin^2 \omega t$. When both Rabi frequencies Ω_1 and Ω_2 are of roughly the same value, the fidelity-reducing term $\propto t^2$ becomes less relevant compared to the term $\propto \sin^2 \omega t$. This can be observed in Fig. 3, where the average fidelity exhibits an oscillatory behavior for a few full rotations around the given axis. The fidelity oscillations become dominated by the $\propto t^2$ decay for longer interaction times.

The average fidelity depends not only on time (duration of the laser pulse), it also depends on the detuning and the Rabi frequencies, since they affect the interaction strength and rotation axis of the applied pulse. The density plot in Figs. 4 and 5 shows the dependence of the average fidelity calculated using the effective model on the Rabi frequencies. The calculations were done for a fixed time duration of 50 ps, which corresponds to a different rotation angle depending on the two Rabi frequencies. Figure 4a shows the dependence of the average fidelity on the two Rabi frequencies. The average fidelity increases as the Rabi frequencies grow, since it increases the interaction energy ω and shortens the time needed to perform certain rotations. What is remarkable here is the strong enhancement of the fidelity (up to unity) in the region where $\Omega_1 = \Omega_2$. This means that the average fidelity of a single-spin rotation depends on the rotation axis in addition to the rotation frequency. The rotations around axes perpendicular to the applied magnetic field are the least sensitive to the nuclear spin effects. The cut of the density plot in Fig. 4a for $\Omega_1 = \Omega_2$ is shown in Fig. 4b. As can be seen in both Fig. 4a and b, for small Ω the average fidelity has a constant value and then increases and oscillates. From the formula (13), we have for the average fidelity in the case

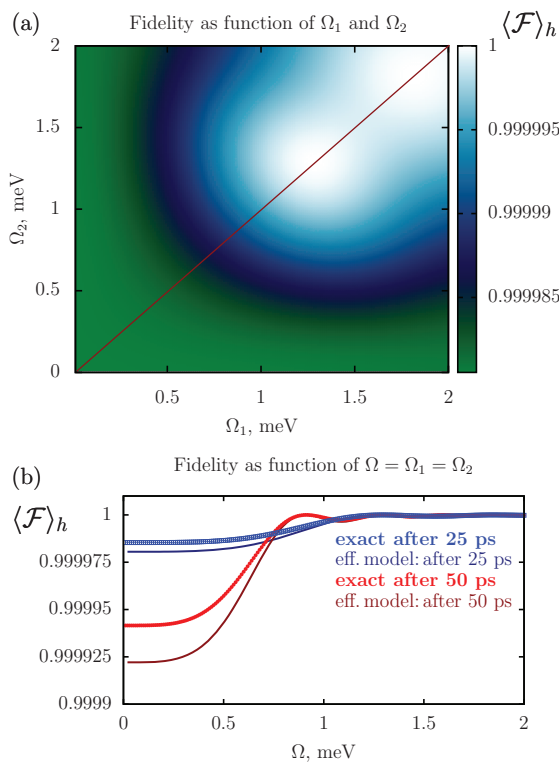


Figure 4 (a) Average fidelity to second order of hyperfine interaction for $\Delta = 10$ meV as function of Rabi frequencies after $t = 50$ ps (calculated by using the effective model). (b) The special case of the average fidelity, when Rabi frequencies are equal ($\Omega_1 = \Omega_2 \equiv \Omega$) as function of Ω at $\Delta = 10$ meV for different interaction times: 25 ps (blue) and 50 ps (red). We include also the exact average fidelity for both interaction times.

$\Omega_1 = \Omega_2 \equiv \Omega$ and under the assumption that $\Omega \ll \Delta$:

$$\langle \mathcal{F} \rangle_h \approx 1 - \frac{2}{3} \frac{\Delta^2}{\Omega^4} \sigma^2 \sin^2 \frac{\Omega^2 t}{2\Delta}. \quad (14)$$

For $\Omega \geq \sqrt{2\Delta/t}$, the fidelity oscillates with decreasing period and for $\Omega \ll \sqrt{2\Delta/t}$ (for $t = 50$ ps and $\Delta = 10$ meV this threshold is around 0.5 meV) is given by $\langle \mathcal{F} \rangle_h \approx 1 - \sigma^2 t^2 / 6$, which for $t = 50$ ps is $\langle \mathcal{F} \rangle_h \approx 0.999927$ and for $t = 25$ ps is $\langle \mathcal{F} \rangle_h \approx 0.999982$. The last expression describes the average fidelity to second order of hyperfine interaction for an electron spin interacting just with a static magnetic field and nuclear spins. As is shown in Fig. 4b, this fidelity increases for shorter interaction times.

The behavior of the average fidelity for spin rotations at $\Omega_1 = \Omega_2$ has a special character: it reaches unity when $\sin \omega t = 0$. This phenomenon is due to the overlap of two effects. Without nuclear spins this situation corresponds to a rotation around an axis in the y - z plane, but with the hyperfine interaction there is an additional fluctuation of the rotation axis perpendicular to the y - z plane. In the case of $\Omega_1 = \Omega_2$, these fluctuations average to zero. This leads to the result that only the off-diagonal elements of the time-evolution operator

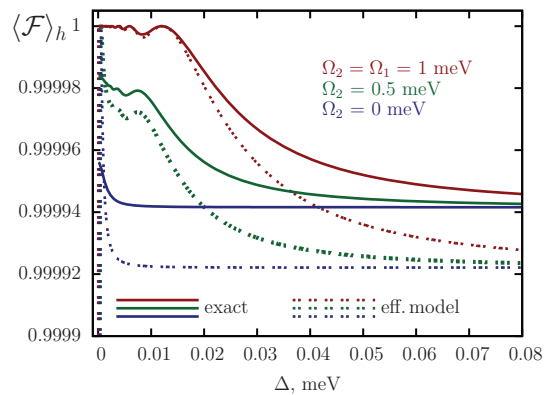


Figure 5 Average fidelity after 50 ps interaction time as a function of the laser detuning for different Rabi frequencies: the red plot shows the special case $\Omega_1 = \Omega_2 = 1$ meV, the green plot shows the average fidelity for $\Omega_1 = 1$ meV, $\Omega_2 = 0.5$ meV, and blue stands for $\Omega_1 = 1$ meV, $\Omega_2 = 0$ meV.

are altered by the hyperfine interaction. But exactly this effect cannot be captured by the fidelity, when $\sin \omega t = 0$, because in this case the ideal time-evolution operator is the identity operator. Consequently, the trace of the product of the time-evolution operators, the ideal one and the one with hyperfine interaction, does not contain the off-diagonal terms of the affected time-evolution operator, which results in a perfect fidelity. This can also be seen in the dependence of the fidelity on the laser detuning in Fig. 5. For equal Rabi frequencies, the fidelity oscillates with increasing period and reaches unity again for $\sin \omega t = 0$.

Figure 5 shows the dependence of the average fidelity on the laser detuning Δ calculated using the effective and the exact models. The curves calculated using the effective model show the same behavior as the ones from the exact calculations and decrease to the same value of ~ 0.99992 for a large value of laser detuning for different combinations of Ω_1 and Ω_2 . However, the exact curves decrease to a slightly different fidelity value of ~ 0.99994 for large Δ . As we can see, the fidelity of single-spin rotations can be increased by using smaller laser detunings. However, this strategy is not optimal because, by decreasing the laser detuning, we increase the population probability of the trion state, which otherwise can be assumed to be only virtually populated. Spontaneous relaxation of the trion state represents a fast relaxation mechanism that will lead to further decrease of fidelity for single-spin rotations in the case of non-negligible trion population. The trade-off of sufficiently large laser detuning for negligible trion state population is not a serious limitation concerning the quantum computation because, even for large Δ , the average fidelity is given by $\langle \mathcal{F} \rangle_h > 0.9999$ for different combinations of Ω_1 and Ω_2 after 50 ps interaction time (see Fig. 5).

The calculated fidelities correspond to small average errors for the single-spin rotations, which are hard to observe experimentally. These fidelities will become relevant as soon as the rotation fidelities describing the laser imperfec-

tions and heavy-light hole mixing (currently estimated to be around 96% [11]) will be overcome. Assuming that the spin-state initialization errors are on the order of 1% [15], the errors of the spin rotations should be on the order of 10% to be measured in an experiment. The minimal average fidelity was found for the case of equal Rabi frequencies in the limit $\Omega_1, \Omega_2 \rightarrow 0$. In this case, the average fidelity is given by $1 - \sigma^2 t^2 / 6$, which means that the average fidelity will sink to 0.9 at $t = 1.8$ ns. The Rabi frequencies in this case should satisfy $\Omega_1, \Omega_2 \ll \sqrt{2\Delta/t}$ according to Eq. (14). For $\Delta = 10$ meV, one requires $\Omega_1, \Omega_2 \ll 0.1$ meV, which is experimentally feasible.

5 Conclusions We studied the nuclear spin effect on the performance of Raman-assisted optical transitions of an electron spin in a semiconductor quantum dot. It was shown that the average rotation fidelities obtained using second-order perturbation theory are in good agreement up to the nanosecond time scale with the numerically averaged fidelities. The average fidelities were calculated for different rotation axes using both approaches. In the framework of the formalism used for describing the interaction of the single electron spin with the laser light, the average rotation fidelities differ strongly for different rotation axes. While the rotations around axes in the $y-z$ plane, perpendicular to the applied magnetic field, suffer least under interaction with nuclear spins, the rotations around the x -axis, which is parallel to the external magnetic field, are the most affected by the hyperfine interaction.

Acknowledgements We gratefully acknowledge funding from the DFG within SPP1285 “Spintronics” and SFB 767, and from BMBF under the program QuaHL-Rep.

References

- [1] D. Loss and D. P. DiVincenzo, Phys. Rev. A **57**, 120 (1998).
- [2] D. P. DiVincenzo, Phys. Rev. A **51**, 1015 (1995).
- [3] G. Burkard, D. Loss, and D. P. DiVincenzo, Phys. Rev. B **59**, 2070 (1999).
- [4] A. Imamoğlu, D. D. Awschalom, G. Burkard, D. P. DiVincenzo, D. Loss, M. Sherwin, and A. Small, Phys. Rev. Lett. **83**(20), 4204 (1999).
- [5] J. R. Petta, A. C. Johnson, J. M. Taylor, E. A. Laird, A. Yacoby, M. D. Lukin, C. M. Marcus, M. P. Hanson, and A. C. Gossard, Science **309**, 2180 (2005).
- [6] F. H. L. Koppens, C. Buizert, K. J. Tielrooij, I. T. Vink, K. C. Nowack, T. Meunier, L. P. Kouwenhoven, and L. M. K. Vandersypen, Nature **442**, 766 (2006).
- [7] V. Cerletti, W. A. Coish, O. Gywat, and D. Loss, Nanotechnology **16**, R27 (2005).
- [8] R. Hanson, J. R. Petta, S. Tarucha, and L. M. K. Vandersypen, Rev. Mod. Phys. **79**, 1217 (2007).
- [9] Ch. Kloeffel and D. Loss, Annu. Rev. Condens. Matter Phys. **4**, 51 (2013).
- [10] P. Chen, C. Piermarocchi, L. J. Sham, D. Gammon, and D. G. Steel, Phys. Rev. B **69**, 075320 (2004).
- [11] S. E. Economou, L. J. Sham, Y. Wu, and D. G. Steel, Phys. Rev. B **74**, 205415 (2006).
- [12] S. E. Economou, Phys. Rev. B **85**, 241401(R) (2012).
- [13] Y. Wu, I. M. Piper, M. Ediger, P. Brereton, E. R. Schmidgall, P. R. Eastham, M. Hugues, M. Hopkinson, and R. T. Phillips, Phys. Rev. Lett. **106**, 067401 (2011).
- [14] S. E. Economou and T. L. Reinecke, Phys. Rev. Lett. **99**, 217401 (2007).
- [15] M. Atatüre, J. Dreiser, A. Badolato, A. Högele, K. Karrai, and A. Imamoğlu, Science **312**, 551 (2006).
- [16] M. H. Mikkelsen, J. Berezovsky, N. G. Stoltz, L. A. Coldren, and D. D. Awschalom, Nature Phys. **3**, 770 (2007).
- [17] J. Berezovsky, M. H. Mikkelsen, N. G. Stoltz, L. A. Coldren, and D. D. Awschalom, Science **320**, 349 (2008).
- [18] D. Press, T. D. Ladd, B. Zhang, and Y. Yamamoto, Nature **456**, 218 (2008).
- [19] F. Dubin, M. Combescot, G. K. Brennen, and R. Melet, Phys. Rev. Lett. **101**, 217403 (2008).
- [20] X. Xu, B. Sun, P. R. Berman, D. G. Steel, A. S. Bracker, D. Gammon, and L. J. Sham, Nature Phys. **4**, 692 (2008).
- [21] A. Ramsay, S. Boyle, R. Kolodka, J. Oliveira, J. Skiba-Szymanska, H. Liu, M. Hopkinson, A. Fox, and M. Skolnick, Phys. Rev. Lett. **100**, 197401 (2008).
- [22] V. Loo, L. Lanco, O. Krebs, P. Senellart, and P. Voisin, Phys. Rev. B **83**, 033301 (2011).
- [23] R.-B. Liu, W. Yao, and L. J. Sham, Adv. Phys. **59**(5), 703 (2010).
- [24] W. B. Gao, P. Fallahi, E. Togan, J. Miguel-Sánchez, and A. Imamoğlu, Nature **491**, 426 (2012).
- [25] J. R. Schaibley, A. P. Burgers, G. A. McCracken, L.-M. Duan, P. R. Berman, D. G. Steel, A. S. Bracker, and D. Gammon, Phys. Rev. Lett. **110**(16), 167401 (2013).
- [26] J. D. Plumhof, R. Trotta, V. Krápek, E. Zallo, P. Atkinson, S. Kumar, A. Rastelli, and O. G. Schmidt, Phys. Rev. B **87**, 075311 (2013).
- [27] A. V. Khaetskii, D. Loss, and L. Glazman, Phys. Rev. Lett. **88**, 186802 (2002).
- [28] W. A. Coish and D. Loss, Phys. Rev. B **70**, 195340 (2004).
- [29] W. A. Coish and J. Baugh, Phys. Status Solidi B **246**, 2203 (2009).
- [30] D. Stepanenko, G. Burkard, G. Giedke, and A. Imamoğlu, Phys. Rev. Lett. **96**, 136401 (2006).
- [31] M. Issler, E. Kessler, G. Giedke, S. Yelin, I. Cirac, M. Lukin, and A. Imamoğlu, Phys. Rev. Lett. **105**, 267202 (2010).
- [32] X. Xu, W. Yao, B. Sun, D. G. Steel, A. S. Bracker, D. Gammon, and L. J. Sham, Nature **459**, 1105 (2009).
- [33] H. Bluhm, S. Foletti, D. Mahalu, V. Umansky, and A. Yacoby, Phys. Rev. Lett. **105**, 216803 (2010).
- [34] B. Sun, C. M. E. Chow, D. G. Steel, A. S. Bracker, D. Gammon, and L. J. Sham, Phys. Rev. Lett. **108**, 187401 (2012).
- [35] M. A. Nielsen and I. L. Chuang, Quantum Computation and Quantum Information (Cambridge University Press, Cambridge, UK, 2009).
- [36] J. Hildmann and G. Burkard, Phys. Rev. B **84**, 205127 (2011).
- [37] L. Pedersen, N. Moller, and K. Molmer, Phys. Lett. A **367**, 47 (2007).
- [38] J. Ghosh and M. R. Geller, Phys. Rev. A **81**, 052340 (2010).